CHAPTER 14

Mechanisms and Models of Nuclear Reactions

Contents

The variety and complexity or nuclear reactions make this a fascinating area of research quite apart from the practical value of understanding fusion and fission. From studies of such properties as the relative amounts of formation of various competing products, the variation of the yields of these with bombarding energy, the directional characteristics and kinetic energies of the products, etc., we may formulate models of nuclear reaction mechanisms. Such models lead to systematics for nuclear reactions and make possible predictions of reactions not yet investigated.

14.1. The reaction cross-section

The probability for a nuclear reaction is expressed in terms of the *reaction cross-section*. The geometric cross-section that a nucleus presents to a beam of particles is πr^2. If we use 6×10^{-15} m as an average value for the nuclear radius, the value of πr^2 becomes $3.14 \ (6 \ \times 10^{-15})^2 \approx 10^{-28}$ m^2. This average geometric cross-section of nuclei is reflected in the unit of reaction probability which is the *barn*, where 1 b $= 10^{-28}$ m^2.
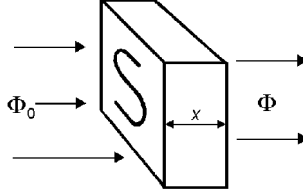
FIG. 14.1. Reduction of particle flux by absorption in a target.

Consider the bombardment of a target containing N_v atoms per m^3 by a homogeneous flux ϕ_o of particles (Fig. 14.1). The flux is expressed in units of particles m^{-2} s^{-1}. The target atoms N_v refer only to the atoms of the species involved in the nuclear reaction. If a Li-Al alloy is bombarded to induce reactions with the lithium, N_v is the number of lithium atoms per m^3 in the alloy, not the total of lithium and aluminum atoms. The change in the flux, $d\phi = \phi - \phi_o$, may be infinitesimal as the particles pass through a thin section of target thickness dx. This change depends on the number of target atoms per unit area (i.e. $N_v dx$), the flux ($\phi_o \approx \phi$), and the reaction cross-section σ.

$$-d\phi = \phi \, \sigma \, N_v \, dx \qquad (14.1)$$

The negative sign indicates that the flux decreases upon passing through the target due to reaction of the particles with the target atoms: thus $-d\phi$ is the number of reactions. Integration gives:

$$\phi = \phi_o \, e^{-\sigma \, N_v \, x} \qquad (14.2)$$

where ϕ_o is the projectile flux striking the target surface. For targets which have a surface area of S (m^2) exposed to the beam, for the irradiation time t, the total number of nuclear reactions ΔN is:

$$\Delta N = (\phi_o - \phi) \, S t \equiv \phi_o \, S t (1 - e^{-\sigma \, N_v \, x}) \qquad (14.3)$$

For a thin target in which the flux is not decreased appreciably upon passage through the target, i.e. $\sigma \, N_v \, x \ll 1$ and hence $e^{-\sigma \, N_v \, x} \approx 1 - \sigma \, N_v \, x$, (14.3) can be reduced to:

$$\Delta N = \phi_o \, S t \sigma \, N_v \, x = \phi_o \, \sigma \, t N_v \, V = \phi_o \, \sigma \, t N_t \quad \text{(thin target)} \quad (14.4)$$

where $V = Sx$ is the target volume, and $N_t = N_v \, V$ is the number of target atoms. Notice that as a result of the product Sx, which equals the volume of the target, the relationship on the right of (14.4) is independent of the geometry of the target and involves only the total number of atoms in it.

Equation (14.4) can be used only when particle fluxes are homogeneous over the whole irradiated sample. In nuclear reactors, where the area of the sample is much smaller than the area of the flux, it is convenient to express the flux in terms of neutrons m^{-2}s^{-1} and the target in terms of total number of atoms, as above.

By contrast, in an accelerator the target surface is often larger than the cross-section of the ion beam, and (14.4) cannot be used without modification. For accelerators the beam intensity (i.e. particle current) I_o (particles s^{-1}) is given by (13.3); 1 A corresponds to $6.24 \times 10^{18} z^{-1}$ charged particles s^{-1}, where z is the charge in electron units on the particle, e.g. 2 for He^{2+}. In (14.4) $\phi_o S$ must be substituted by $6.24 \times 10^{18} iz^{-1}$, where i (A) is the electric current.

In (14.4) $N_v x$ has the dimensions of atoms m^{-2}. This is a useful quantity in many calculations and for a pure elemental target is equal to

$$N_v x = 1000 \, \mathbf{N}_A \, \rho \, x \, y_i / M \tag{14.5}$$

where ρ is the density of the target (kg m^{-3}), M the atomic weight (in *gram* mole) of the element, x the target thickness in m, and y_i the isotopic fraction of reactive atoms of kind i in the target.

As an example of the use of these equations, consider the irradiation of a gold foil by thermal neutrons. Assume the foil is 0.3 mm thick with an area of 5 cm^2 and the flux is 10^{17} n m^{-2} s^{-1}. The density of gold is 19.3 g cm^{-3} while the cross-section for the capture of thermal neutrons by ^{197}Au is 99 b. Transferring these units into SI and introducing them into (14.3) for an irradiation time of 10 min yields a value of 4.6×10^{15} for the number of ^{198}Au nuclei formed. If the thin target equation is used (14.4), the value of 5.0×10^{15} nuclei of ^{198}Au is obtained. If the same gold foil is bombarded in a cyclotron with a beam of protons of 1 μA when the cross-section is 1 b and $t = 10$ min, the number of reactions is 6.6×10^{12}.

Frequently, the irradiated target consists of more than one nuclide which can capture bombarding particles to undergo reaction. The *macroscopic* cross-section, which refers to the total decrease in the bombarding particle flux, reflects the absorption of particles by the different nuclides in proportion to their abundance in the target as well as to their individual reaction cross-sections. Assuming that the target as a whole contains N_v atoms m^{-3} with individual abundances y_1, y_2, etc., for nuclides 1, 2, etc., the individual cross-sections are σ_1, σ_2, etc. The macroscopic cross-section Σ (m^{-1}) is

$$\Sigma = N_v \sum_1^n y_i \sigma_i \tag{14.6}$$

For a target which is x m thick one obtains

$$\phi = \phi_o \, e^{-\Sigma x} \tag{14.7}$$

The value Σ^{-1} is the average distance a projectile travels between successive collisions with the target atoms (the *mean free path*).

14.2. Partial reaction cross-sections

The irradiation of a target may lead to the formation of a number of different products. For example, the irradiation of ^{63}Cu with protons can produce the nuclides ^{62}Zn, ^{63}Zn, ^{62}Cu, all of which are radioactive:

$$^{63}\text{Cu} + {}^{1}\text{H} \rightarrow \begin{cases} (\text{p,n}) & {}^{63}\text{Zn} + \text{n} \\ (\text{p,2n}) & {}^{62}\text{Zn} + 2\text{n} \\ (\text{p,pn}) & {}^{62}\text{Cu} + {}^{1}\text{H} + \text{n} \end{cases}$$

The formation probability of each product corresponds to a *partial reaction cross-section*. The total reaction cross-section σ_{tot} is the sum of all the partial cross-sections and measures the probability that the projectile causes a nuclear reaction independent of the products formed. Thus, the decrease in intensity of the particle flux is proportional to σ_{tot}. The amount of an individual product formed is proportional to σ_i, where σ_i corresponds to the partial reaction cross-section for the formation of the *i*:th product.

Some partial cross-sections have their own names such as the *scattering cross-section* for elastic and inelastic scattering (σ_{scat}), the *activation cross-section* (σ_{act}) for the formation of radioactive products, the *fission cross-section* (σ_f) for fission processes, and *adsorption* or *capture cross-sections* (σ_{abs} or σ_{capt}) for the absorption or capture of particles. If all of these processes take place, one obtains (with caution to avoid overlapping reactions)

$$\sigma_{\text{tot}} = \sigma_{\text{scat}} + \sigma_{\text{act}} + \sigma_f, \text{ etc} \qquad (14.8)$$

In the irradiation of ^{235}U with thermal neutrons, σ_{scat} is about 10 b, σ_{act} (for forming ^{236}U) is approximately 107 b, and σ_f is 582 b.

The reaction cross-section depends on the projectile energy as shown in Figure 14.2. The curves obtained for the partial reaction cross-section as a function of projectile energy are known as *excitation functions* or *excitation curves.*

14.3. Resonance and tunneling

Experimentally, it is found that nuclear reactions sometimes occur at energies less than that required by the Coulomb barrier. This behavior is related to the wave mechanical nature of the particles involved in a nuclear reaction.

As a projectile approaches a target nucleus in a nuclear reaction, the probability that there will be overlap and hence interaction in their wave functions increases. This concept was used in §11.7.3 to explain the emission of α-particles with energies less than that required by the Coulomb barrier height. Such tunneling may also occur for projectiles approaching the nucleus from the outside. An example is provided by the reaction of protons with lithium (Fig. 14.3).

$$^{7}_{3}\text{Li} + {}^{1}_{1}\text{H} \rightarrow {}^{8}_{4}\text{Be}^{*} \rightarrow \begin{cases} 2\,{}^{4}_{2}\text{He} & Q = 17.4 \text{ MeV} \quad (a) \\ {}^{8}_{4}\text{Be} + \gamma & Q = 17.2 \text{ MeV} \quad (b) \\ {}^{7}_{4}\text{Be} + \text{n} & Q = -1.64 \text{ MeV} \quad (c) \end{cases}$$

For this reaction the value of $E_{\text{cb(min)}}$ is 1.3 MeV. However, due to tunneling the reactions begin to occur at lower proton energies. At an energy of 0.15 MeV about 0.1% of the protons penetrate the Coulomb barrier, at 0.3 MeV about 1%, and at 0.6 MeV about 20%.

FIG. 14.2. Excitation functions for reactions between ^{4}He ions and ^{54}Fe target nuclei. The kinetic energy of the projectile is in the laboratory system. (From Houck and Miller.)

The reaction cross-section is closely related to the excited energy states of the compound nucleus. Four such levels are shown for ^{8}Be* in Figure 14.3. To the left of the figure the (p,γ), (p,n) and (p,α) partial cross-sections (excitation functions) are shown as function
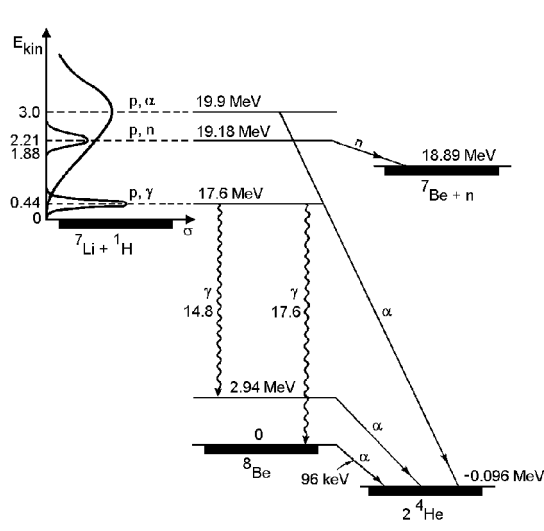
FIG. 14.3. Yield curves for the reaction between protons and ^{7}Li, leading to different excited levels in ^{8}Be, followed by decay to stable end products.

of the proton kinetic energy. The maximum cross-section for reaction (b) occurs at a proton kinetic energy of 0.44 MeV, which, together with the Q-value, 17.2 MeV, of the reaction ^{7}Li + ^{1}H → ^{8}Be, leads to an excitation energy of 17.6 MeV, which exactly matches an excited level of the same energy in ^{8}Be*. At an excitation energy of 19.18 MeV another energy level is reached in the compound nucleus leading to its decay into ^{7}Be + n, reaction (c). The excitation energy is achieved from the release of nuclear binding energy (17.25 MeV) and from the proton kinetic energy. The amount needed is 19.18 – 17.25 = 1.93 MeV. In order to conserve momentum, the proton must have (8/7) × 1.93 = 2.21 MeV in kinetic energy. The increase in cross-section when the total excitation energy matches an excited energy level of the compound nucleus is known as a *resonance*.

   This particular reaction is of interest for several reasons. It was the first nuclear reaction that was produced in a laboratory by means of artificially accelerated particles (Cockcroft and Walton 1932; cf. §13.3). Reaction (b) is still used for the production of γ-radiation (17 MeV), while reaction (c) is used as a source of mono-energetic neutrons. The energy of the neutrons from reaction (c) is a function of the proton energy and the angle between the neutron and the incident proton beam. A necessary requirement, however, is that the threshold energy (1.64 × (8/7) = 1.88 MeV) must be exceeded, the Q-value for reaction (c) being –1.64 MeV.

14.4. Neutron capture and scattering

   Unlike charged particles, no Coulomb barrier hinders neutrons from reaching the target nucleus. This leads to generally higher reaction cross-sections for neutrons, particularly at very low energies. Moreover, since neutrons can be produced in very high fluxes in nuclear reactors, neutron-induced processes are among the more important nuclear reactions.

   We have seen that the geometric cross-section of a target nucleus is in the order of 1 b, or 10^{-28} m^2. Experimentally, the cross-sections for capture of energetic ("fast") neutrons ($\geq$ 1 MeV) are often close to 1 b. However, for neutrons whose kinetic energy is in the 1 – 100 eV region, some nuclei show very large cross-sections — as high as 10^5 b. Such values can be explained as being due to neutron capture where the compound nucleus is excited exactly to one of its discrete energy levels (resonance capture). This does not mean that the nucleus is larger than its calculated geometric cross-section but that the interaction probability is very large in such cases — greater than the calculation of πr^2 would indicate.

   For low energy ("slow") neutrons ($\ll$ 1 MeV) the cross-section is also larger than the πr^2 value, and decreases as the velocity increases; this relation, $\sigma \propto v^{-1}$, is shown for boron in Figure 14.4. The relationship between the cross-section and the neutron velocity can be understood in wave mechanical terms since the wavelength associated with the neutron increases with a decrease in velocity. According to the matter-wave hypothesis (§10.4) the wavelength associated with a moving particle is $\lambda = $ /(mv) which can be written:

$$\lambda = (2mE_{\text{kin}})^{-\frac{1}{2}} = 0.286 \times 10^{-8} (mE_{\text{kin}})^{-\frac{1}{2}} \tag{14.9}$$

While the wavelength of a slow neutron is about 0.1 nm, that of a fast neutron is less than 1/1000 of that. Since the reaction probability increases with increasing particle wavelength, a slow-moving particle has a higher probability of reaction than a faster one of the same
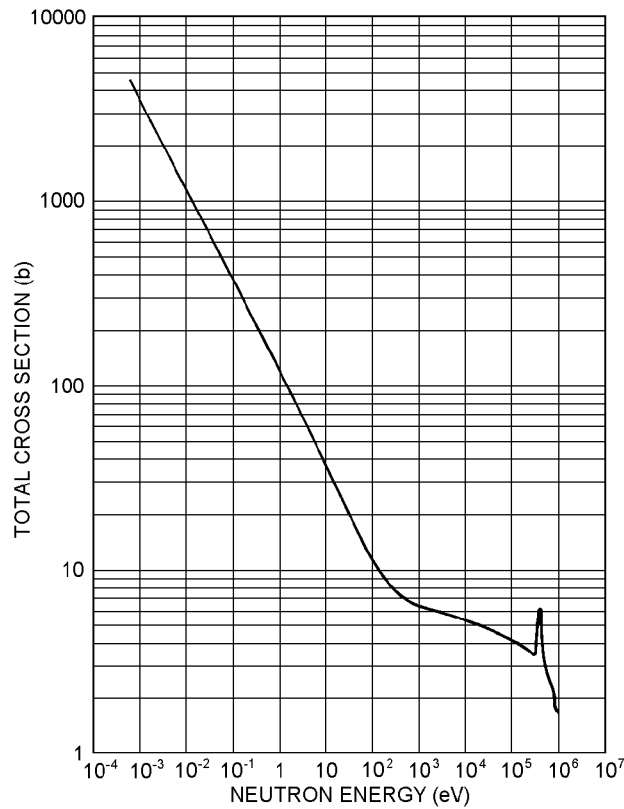
FIG. 14.4. The total reaction cross-section of ^{10}B for neutrons of various kinetic energies.

kind.

 In effect, the wave properties make neutrons appear much larger than their geometric size and increases the probability of interaction with the nucleus. From (14.9) it follows that

$$\sigma_{capt} \propto \lambda_n \propto E_n^{-\frac{1}{2}} \propto v_n^{-1} \tag{14.10}$$

where λ_n, E_n, and v_n are the wavelength, kinetic energy, and velocity, respectively, of the neutron. This relation is known as the $1/v$ *law*. This law is valid only where no resonance absorption occurs. In Figure 14.4 $\sigma_{tot} = \sigma_{capt} + \sigma_{scat}$, but σ_{scat} is approximately constant. Since σ_{capt} decreases as E_n increases, at higher energies (≥ 500 eV) σ_{scat} dominates over σ_{capt}, except for the resonance at 0.3 MeV. The capture or neutrons in ^{10}B leads to the formation of ^{7}Li and ^{4}He.

14.5. Neutron diffraction

  From (14.9) we calculated that for neutrons the wavelength at thermal energies is on the order of 0.1 nm, i.e. of the same order of magnitude as the distance between atomic planes

in a crystal. Thermal neutrons can, therefore, be scattered by crystals in the same manner as X-rays. For studies of crystal structures by neutron diffraction, a beam of mono-energetic neutrons can be obtained from the spectrum of neutron energies in a reactor by the use of monochromators.

The probability of scattering of neutrons without energy change (*coherent scattering*) is approximately proportional to the area of the nucleus. As a consequence, coherent scattering of neutrons is less dependent on the atomic number than the scattering of X-rays which is proportional to the electron density (i.e. $\propto Z^2$). As a result of this difference, for a compound consisting of both heavy and light atoms, the position of the lighter atoms can be more easily determined using neutron diffraction, while X-ray diffraction is better for locating the heavier atoms. Neutron diffraction is, therefore, valuable for complementing the information obtained on the position of heavy atoms by X-ray diffraction. Neutron diffraction is particularly valuable in the location of hydrogen atoms in organic and biological materials.

14.6. Models for nuclear reactions

No single model is successful in explaining all the aspects of the various types of nuclear reactions.

Let us consider three models which have been proposed for explaining the results of nuclear reaction studies.

14.6.1. *The optical model*

In the process of elastic scattering the direction of the particles is changed but none of the kinetic energy is converted to nuclear excitation energy. This would indicate that the reaction is independent of the internal structure of the nucleus and behaves much like the scattering of light from a crystal ball. Consequently, a model has been developed based on the mathematical techniques used in optics. Light shining on a transparent crystal ball is transmitted with some scattering and reflection but no absorption. Light shining on a black crystal ball is all absorbed and there is no transmission or scattering. In nuclear reactions the incoming particles are scattered in elastic scattering and are absorbed in induced transmutations. Therefore, if the nucleus is to act as a crystal ball it can be neither totally transparent nor totally black. The optical model of the nucleus is also known as the *cloudy crystal ball model*, indicating that nuclei both scatter and absorb the incoming particles.

The nucleus is described as a potential well containing neutrons and protons. The equation for the nuclear potential includes terms for absorption and scattering. This potential can be used to calculate the probability for scattering of incident particles and the angular distribution of the scattering. The model is in excellent agreement with experiments for scattering. Unfortunately, this model does not allow us to obtain much information about the consequences of the absorption of the particles which lead to inelastic scattering and transmutation.

14.6.2. *Liquid-drop model*

As the excitation energy of an excited nucleus increases, the energy levels get closer together. Eventually, a continuum is reached where the density of nuclear levels is so great that it is no longer possible to identify individual levels. (This is similar to the case for electronic energy levels of atoms.) When the excited nucleus emits a proton or neutron while in the continuum energy, the resultant nucleus may be still sufficiently energetic that it remains in the continuum region.

N. Bohr has offered a mechanism to explain nuclear reactions in nuclei which are excited into the continuum region. When a bombarding particle is absorbed by a nucleus, the kinetic energy of the bombarding particle plus the binding energy released by its capture provide the excitation energy of the compound nucleus. In this model, the *compound nucleus* becomes uniformly excited in a manner somewhat analogous to the warming of a small glass of water upon addition of a spoonful of boiling water. As the nucleons move about and collide in the nucleus, their individual kinetic energies vary with each collision just as those of molecules in a liquid change in molecular collisions. As this process continues, there is an increase in the probability that at least one nucleon will gain kinetic energy in excess of its binding energy (assuming the total excitation energy to be larger than the binding energy). That nucleon is then evaporated (i.e. leaves the nucleus) analogously to the evaporation of molecules from liquid surfaces.

The evaporation of the nucleon decreases the excitation energy of the residual nucleus by an amount corresponding to the binding energy plus the kinetic energy of the released nucleon. The evaporation process continues until the residual excitation energy is less than the binding energy of a nucleon. The excitation energy remaining at this point is removed from the nucleus by emission of γ-rays.

Assume that the compound nucleus $^{188}_{76}$Os is formed with a total excitation energy of 20 MeV. If the average binding energy of a neutron is 6 MeV and if each neutron leaves with 3 MeV of kinetic energy, evaporation of a neutron de-excites the nucleus by 9 MeV. Therefore evaporation of two neutrons would leave the residual ^{186}Os nucleus with an excitation energy of only 2 MeV. Since this is below the binding energy of a neutron, further evaporation is not possible and γ-ray emission removes the final 2 MeV. If the ^{188}Os compound nucleus was formed by α-bombardment of ^{184}W, the reaction is represented as

$$^{184}_{74}\text{W} + \alpha \rightarrow [^{188}_{76}\text{Os}]^* \rightarrow {}^{186}_{76}\text{Os} + 2\text{n}$$

14.6.3. *Lifetime of the compound nucleus*

An important assumption of the compound nucleus theory is that the nucleon system is held together long enough for the energy to be shared by all nucleons. Furthermore, it is assumed that the time it takes for the accumulation on one nucleon of enough energy to allow evaporation is even longer by nuclear standards. This time is of the order of 10^{-14} s as compared to a time of 10^{-20} s required for a nucleon to cross the nuclear diameter once. Since the time is so long and there are so many inter-nucleon collisions, the nucleus retains no pattern ("no memory") of its mode of formation, and the mode of decay should

therefore be independent of the mode of formation and only depend on the amount of excitation energy, the *nuclear temperature* (usually expressed in MeV). For example, ^{150}Dy ($t_{1/2}$ = 7.2 min) can be formed in the following two ways:

$$\left. \begin{array}{l} ^{12}_{6}\text{C} + \ ^{144}_{60}\text{Nd} \\ \\ ^{20}_{10}\text{Ne} + \ ^{136}_{56}\text{Ba} \end{array} \right\} \quad \rightarrow \quad [^{156}_{66}\text{Dy}^*] \rightarrow \quad ^{150}_{66}\text{Dy} + 6n$$
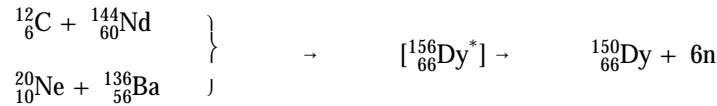
both form the excited ^{156}Dy*. To a first approximation, the probability for formation of ^{150}Dy is dependent only on the excitation energy of the compound nucleus ^{156}Dy* but not on the manner in which this compound nucleus is formed (Fig. 14.5). This assumption of no memory of the mode of formation is not valid if very different amounts of angular momenta are involved in different modes of formation or the collision energy is very high. For example, for proton induced reactions, the excitation energy is essentially all available for internal (nucleon) excitation. By contrast, as heavier bombarding particles are used, the average angular momentum of the compound system increases and the excitation energy is divided between the rotation and internal (nucleon) excitation. The modes of subsequent decay of the compound nucleus is affected by the amount of excitation energy that was involved in the angular momentum of the compound nucleus.

In general, neutron emission is favored over proton emission for two reasons. First, since there are usually more neutrons than protons in the nucleus, a neutron is likely to accumulate the necessary evaporation energy before a proton does. Second, a neutron can depart from the nucleus with a lower kinetic energy — the average neutron kinetic energy is 2 – 3 MeV. On the other hand, evaporating protons must penetrate the Coulomb barrier, so they often need about 5 MeV above their binding energy. It takes, as an average, a
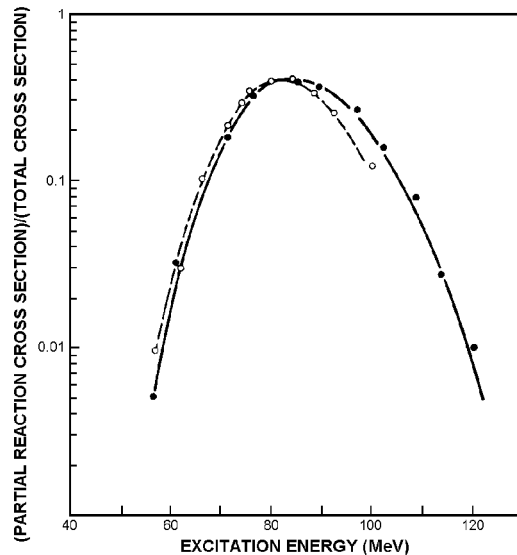
FIG. 14.5. Excitation functions for the formation of ^{150}Dy, through bombardment of either ^{144}Nd with ^{12}C ( ) or ^{136}Ba with ^{20}Ne ( ). (From Lefort)

longer time for this amount ($\sim$ 12 MeV *vs.* $\sim$ 9 MeV for neutrons) to be concentrated on one nucleon.

Obviously, such a simple picture ignores a large number of complicating effects that can, in particular cases, reverse the order of these cross-sections. Nevertheless, despite its simplicity, the compound nucleus theory has been of great value in explaining many aspects of medium energy nuclear reactions (i.e. 10 MeV per nucleon of the bombarding particle).

14.6.4. *Direct interaction model*

The compound nucleus theory assumes that the bombarding projectile interacts with the nucleus as a whole. The nucleus is excited uniformly and evaporation of low energy nucleons follows. This model fails to explain some of the phenomena observed as the kinetic energy of the bombarding particle increases. One such observation is the occurrence of high energy neutrons and protons among the emitted particles. Another is the large cross-sections for reactions such as $X_1(p,pxn)X_2$ at energies where 6 or 7 nucleons are evaporated in order to de-excite the nucleus. At still higher energies compound nucleus formation is too slow to occur at all and the target nucleus (and also projectile in case of heavy ions) splits rapidly into several fragments.

Figure 14.6 shows the cross-section for production of nuclides of $A =$ 20 – 200 when ^{208}Pb is bombarded with protons of energies 40, 480, and 3000 MeV. Such reactions, yielding a large number of products at high projectile energies, have been extensively studied by nuclear chemists, partly because the mixture of products required separation by radiochemical techniques. Although some ambiguity exists in its use, the term *spallation* is often used for reactions in which a number of particles are emitted as a result of a direct interaction. At very high energies, not only is a broad range of products formed but the probability for the formation of these products is, within an order of magnitude, similar for every mass number, except around the projectile and target masses where strong peaks occur (Fig. 14.7). Further, studies at bombarding energies above 100 MeV/u show that high energy protons, neutrons, and heavier particles are emitted from the nucleus in a forward direction. Compound nucleus evaporation would be expected to be isotropic (i.e. show no directional preference in the center-of-mass system).

Serber has suggested a mechanism that satisfactorily accounts for many features of nuclear reactions at bombardment energies above 50 MeV for protons, deuterons, and α-particles. At such energies the relative speed between projectile and target nuclei is so high (near **c**) that the time available for distribution of energy between all nucleons is too short and we can initially consider projectile and target nuclei as consisting of fairly isolated nucleons. The concept of a common nuclear temperature is no longer valid. He proposed that high energy reactions occur in two stages.

(i) During the first stage the nucleons in the incoming particle undergoes direct collision with individual target nucleons. In these collisions the struck nucleon often receives energy much in excess of its binding energy. Consequently, after each collision both the nucleon belonging initially to the bombarding particle and the struck nucleon have some probability of escaping the nucleus since their kinetic energies are greater than their binding energies. If both particles escape, the nucleus is usually left with only a small amount of excitation
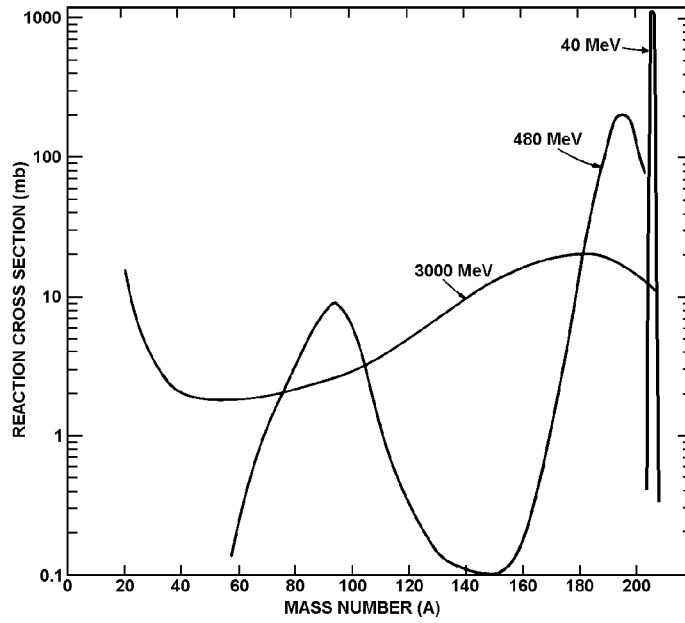
FIG. 14.6. Mass yield curve obtained by bombardment of lead with high energy protons. (From Miller and Hudis.)

energy. This explains the high cross-section for (p,pn) reactions. In support of this explanation, both the emitted proton and neutron have large kinetic energies. Either one or
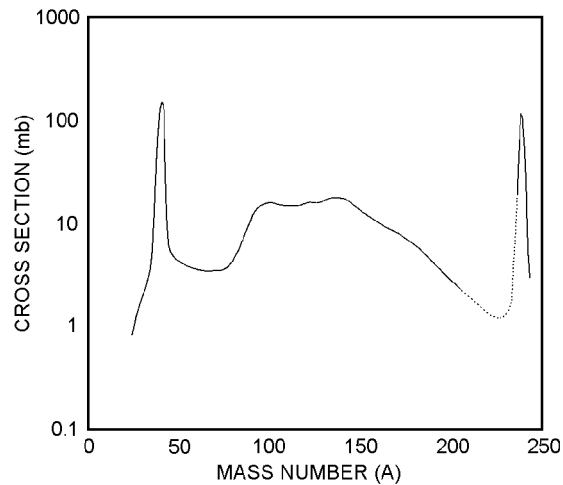
Fig. 14.7. Mass yield curve obtained by bombardment of ^{238}U with ^{40}Ar ions at 7.2 MeV/u. (From Kratz, Liljenzin, Norris and Seaborg.)

both of the original pair may collide with other nucleons in the nucleus rather than escape. During this initial stage, known as the *knock-on-cascade process,* the total number of direct collisions may be one or many. After a period lasting about 10^{-19} s, some of the struck nucleons have left the nucleus.

 (ii) In the remaining nucleus the residual excitation energy is uniformly distributed. The reaction then enters its second and slower stage, during which the residual excitation energy is lost by nucleon evaporation. This stage resembles the compound nucleus process very closely.

 In Figure 14.6 at 40 MeV only the second, evaporation, stage is observed as seen by the narrow mass distribution curve. The curves for 480 and 3000 MeV reflect the increased importance of the first, direct interaction stage which leads to a broad spectrum of product mass numbers.

 The experimental data have been successfully reproduced using a calculation technique known as the Monte Carlo method and assuming a Fermi gas model for the nucleus. This model treats the nucleons like molecules of a very cold ideal gas in a potential well. The nucleons do not follow the Pauli exclusion principle and fill all vacant orbitals.

 In a *Monte Carlo calculation,* the history of each incident nucleon is studied in all its collisions in the nucleus. Each collision with a target nucleon is characterized by probability distributions for occurrence, for energy, for angular distribution, and for pion formation. The outcome of each process is obtained from a series of properly distributed random numbers and scores are accumulated for each process. The calculations are repeated for different impact points. It is the use of random numbers that is the basis of the Monte Carlo technique. Modern computers allow so many random number calculations that a useful pattern of events emerges from the cumulative scores.

 Figure 14.8 shows the quite satisfactory agreement for two bombardment energies between experimental yields of A in proton bombardment of copper (solid lines) and a Monte Carlo calculation (histograms).
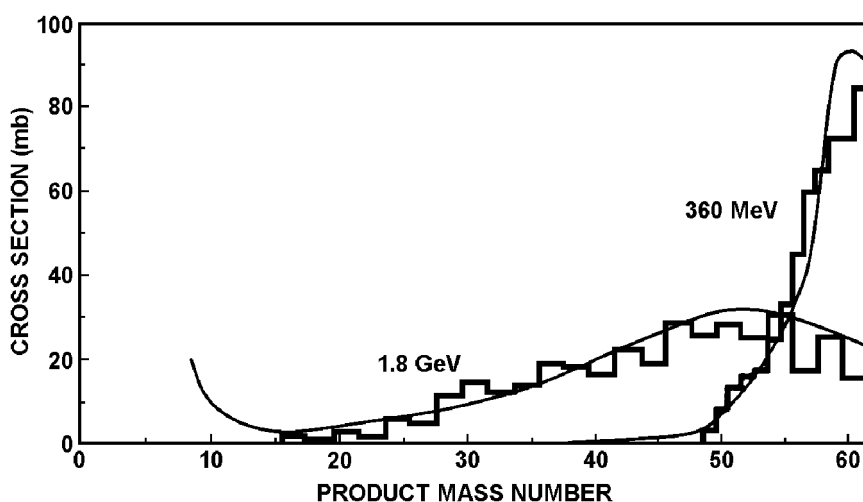
FIG. 14.8. Comparison of mass yield curves for proton interaction with copper as predicted by Monte Carlo calculations (histogram) with experimental results (curve). (From G. Friedlander.)

14.7. Nuclear fission

Nuclear fission is unique among nuclear reactions since the nucleus divides into roughly equal parts with the release of a large amount of energy, about 200 MeV per fission. It is probably no overstatement to say that fission is the most important nuclear process, both for its potential to destroy civilization through the use of weapons and its potential through reactors to supply abundant power for all people.

An aspect of fission which has been studied extensively is the distribution of mass, charge and kinetic energy among the fragments formed in fission. No matter how nuclei are made to undergo fission, fragments of various masses are formed which result in production of chemical elements as light as zinc (atomic number 30) and as heavy as gadolinium (atomic number 64), with half-lives from fractions of seconds to millions of years. Approximately 400 different nuclides have been identified as products in the fission of ^{235}U by neutrons. Study of these fission products has required extensive radiochemical work and continues as a very active field of research – for example, in the measurement of very short-lived products. Although fission is an extremely complicated process, and still challenges theorists, satisfactory models for most of the fission phenomena have been developed.

14.7.1. *Mass and charge distribution*

If fission was symmetric, i.e. if two fragments of equal mass (and charge) were formed, the thermal neutron fission of ^{235}U would lead to the production of two $^{118}_{46}$Pd nuclides,

$$^{235}_{92}\text{U} + \text{n} \rightarrow 2\ ^{118}_{46}\text{Pd}$$
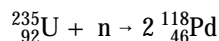
However, a plot showing the amount of different masses formed is a curve with two maxima - one near mass number 97 (close to the n-shell $N = 50$) and a second near mass number 137 (close to the n-shell $N = 82$) (Fig. 14.9). These two masses are formed together in the most probable split which is asymmetric ($A_1 \quad A_2$). As Figure 14.9 shows, symmetric fission ($A_1 = A_2$) is rare in fission of ^{235}U by thermal neutrons — the yield for $A = 115$ is only 0.01% compared to 6% for $A_1 = 97$ (or $A_2 = 137$). Since two fission products are formed in each fission event, mass yield curves like that in Figure 14.9 must total 200% on a number basis.

From the mass yield curve in Figure 14.9 we learn that complementary fission products (i.e. the two products A_1 and A_2 with identical yield values symmetrically located around the minimum) add up to about 234, not 236. Direct neutron measurements reveal that on the average 2.5 neutrons are emitted in fission of ^{235}U by thermal neutrons. This number increases as the Z of the target and as the bombarding energy increases.

Because the N/Z ratio for $^{236}_{92}$U (the fissioning nucleus) is 1.57, while the ratio necessary for stability is 1.2 - 1.4 in the elements produced in fission, fission fragments always have a too large N/Z ratio. This is partially compensated by the emission of several neutrons in the act of fission, *prompt neutrons.* However, the number of neutrons emitted is not sufficient to lower the N/Z ratios to stable values. To achieve further lowering, the fission fragments, after neutron emission, undergo a series of radioactive decay steps in which β^--particles are emitted. Since the β-decay occurs with no change in A, successive β-decay
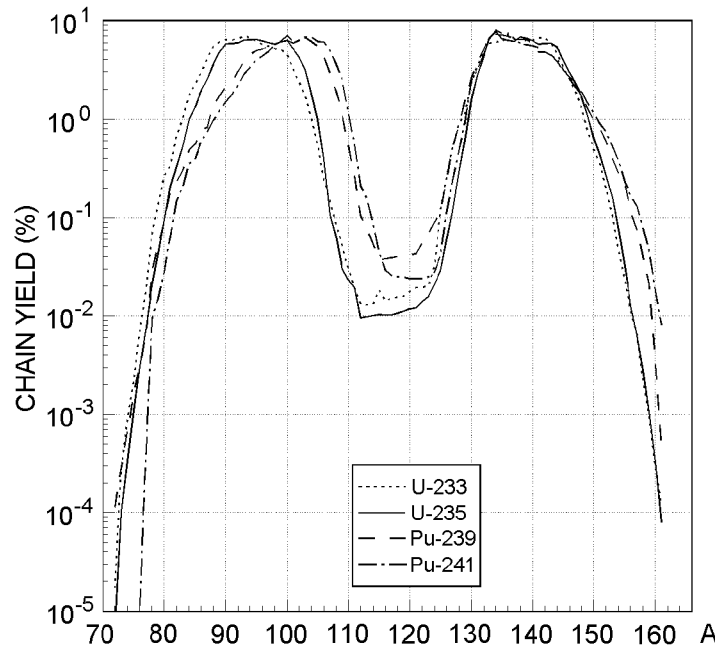
FIG. 14.9. Chain yield curves for fission of ^{233}U, ^{235}U, ^{239}Pu and ^{241}Pu with thermal neutrons.

steps follow the isobar parabola of the stability valley (see Fig. 3.5; cf. also the nuclide chart, Appendix C). For $A = 137$, $^{137}_{52}$Te is the first nuclide measured. The chain sequence is

$$^{137}\text{Te} \xrightarrow{3.5\ s} {}^{137}\text{I} \xrightarrow{24.5\ s} {}^{137}\text{Xe} \xrightarrow{3.82\ min} {}^{137}\text{Cs} \xrightarrow{30.0\ y} {}^{137m}\text{Ba} \xrightarrow{2.6\ m} {}^{137}\text{Ba(stable)}$$
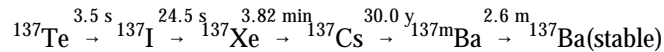
Thermal fission of ^{235}U leads to a yield of 6.183% for the $A = 137$ chain. In a small number of cases the decay chains passes nuclides which emit a neutron after β^--decay, so called *delayed neutrons* (e.g. 0.016% of all neutrons from thermal fission of ^{235}U are delayed neutrons). Neutrons are emitted in 2% of the ^{137}Te β-decays and in 6.4% of the ^{137}I β-decays. The existence of delayed neutrons is important for nuclear reactor control, see Ch. 19.

  In addition to measuring the variation of mass yield, the variation of fission yield in isobaric mass chains as a function of the proton number has been studied. In Figure 14.10, "individual" yield data are presented for the $A = 93$ chain. In general, the charge distribution yields follow a Gaussian curve with the maximum displaced several units below the value of Z for stable nuclides with the same A. For $A = 93$ the yield is largest for $Z = 37$ and 38 (*most probable charge*, Z_p) compared to the stable value of $Z = 41$.

$$y(A,Z) = y(A)\ s^{-1}\ (2\pi)^{-\frac{1}{2}}\ e^{-(Z-Z_p)^2/(2s^2)} \tag{14.11}$$

$\sim 3 \times 10^{-6}\%$ $4 \times 10^{-3}\%$ 0.67% 2.96% 2.66% 0.074% $3 \times 10^{-4}\%$ $\sim 2 \times 10^{-8}\%$

$\Downarrow$ $\Downarrow$ $\Downarrow$ $\Downarrow$ $\Downarrow$ $\Downarrow$ $\Downarrow$ $\Downarrow$

$^{93}_{34}\text{Se}$ $\xrightarrow{?}$ $^{93}_{35}\text{Br}$ $\xrightarrow{?}$ $^{93}_{36}\text{Kr}$ $\xrightarrow{1.3\ s}$ $^{93}_{37}\text{Rb}$ $\xrightarrow{5.8\ s}$ $^{93}_{38}\text{Sr}$ $\xrightarrow{7.45\ min}$ $^{93}_{39}\text{Y}$ $\xrightarrow{10.1\ h}$ $^{93}_{40}\text{Zr}$ $\xrightarrow{1.5\ My}$ $^{93}_{41}\text{Nb}$ (stable)

$\downarrow \beta^- \text{ n}?$ $\downarrow \beta^- \text{ n}$ $\downarrow \beta^- \text{ n } 1.9\%$ $\downarrow \beta^- \text{ n } 1.4\%$

$^{92}_{35}\text{Br}$ $^{92}_{36}\text{Kr}$ $^{92}_{37}\text{Rb}$ $^{92}_{38}\text{Sr}$ Total chain yield $= 6.375\%$
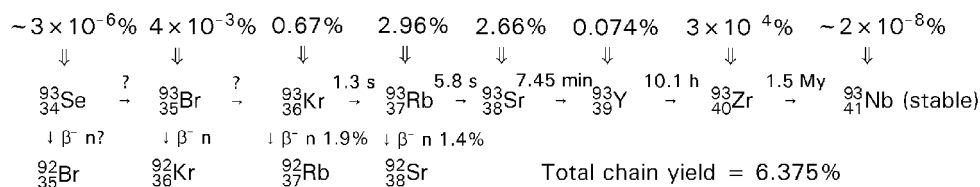
FIG. 14.10. Fission product decay chain of $A = 93$. The independent yields in the upper row refer to nuclides believed to be formed directly in fission of ^{235}U by thermal neutrons.

where $y(A,Z)$ is the initial yield of the fission fragment with mass A and atomic number Z, $y(A)$ the total yield of mass A (usually given in % of all fissions) and s the width parameter for the charge distribution at mass A. Tables of $y(A)$, Z_p and s for fission of several nuclides by thermal and energetic neutrons are available in the literature. Values of $y(A)$, the *chain yield*, for fission of ^{235}U by thermal neutrons are usually also given in nuclide charts.

  Fission of heavy elements other than uranium can be made to occur by particle bombardment, particularly if we use high energy neutrons or high energy charged particles such as protons. The mass distribution curve for this type of fission is interesting. At low bombarding energies it is asymmetric for many heavy elements as it is with low energy neutrons. However, as the energy of bombardment is increased the valley between the peaks of the curve becomes more shallow and, at high energies, a single-humped symmetric curve is obtained (Fig. 14.11). Thus, the most probable mode of mass split changes from asymmetric at low energies to symmetric at high energies. As the energy is increased, the fission yield curve $y(A)$ or cross-section curve $\sigma_{\text{fiss}}(A)$ becomes indistinguishable from yield curves of the type in Figure 14.6 ascribed to direct interaction mechanisms.

  In contrast to the above, low energy fission of nuclei in the radium region results in mass yield curves with three peaks symmetric around $\sim A/2$. Furthermore, low energy or spontaneous fission of some heavy actinide isotopes, e.g. ^{259}Fm, produces symmetric mass yield curves.

  The light mass peak of double-humped fission yield curves shifts towards heavier masses when heavier nuclides undergo fission, but the position of the heavier mass peak remains almost constant. The Z_p-value increases somewhat with increasing charge of the fissioning nucleus. As an example the average mass of the light and heavy mass yield peaks in thermal fission of ^{235}U, ^{239}Pu and ^{241}Pu are 96.57, 100.34, 102.58 and 139.43, 139.66, 139.42 u, respectively, c.f. Fig. 14.9.

14.7.2. *Energy of fission*

  From the curve of the binding energy per nucleon (see Fig. 3.3), we calculated in §3.4 that about 200 MeV would be released in the fission of a heavy element. In this section we consider how this fission energy is partitioned.

  The neutrons emitted have an average kinetic energy of ~ 2 MeV. For the average of 2.5 neutrons emitted in fission of ^{235}U by thermal neutrons, about 5 MeV of the fission energy is required. The emission of γ-rays in the act of fission, *prompt* γ-rays, accounts for another 6 - 8 MeV. The largest part of the fission energy is observed as the kinetic energy
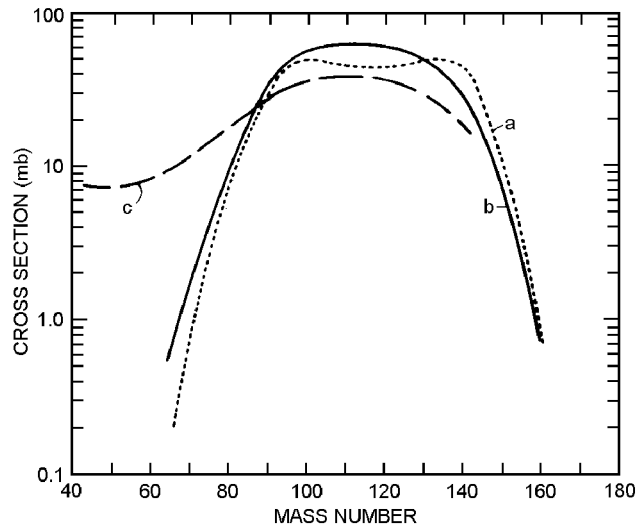
FIG. 14.11. Mass yield curves for fission products from uranium irradiated with protons: (a) 100 MeV, (b) 170 MeV, and (c) 2.9 GeV. (From Friedlander.)

of the fission products. We can estimate this by calculating the Coulombic repulsion energy of a probable fission product pair, $^{93}_{37}$Rb and $^{143}_{55}$Cs. The model used is two touching spherical nuclei with a charge center distance $d = 12.7$ fm (Fig. 14.12a). From (12.15) we calculate that the repulsive Coulomb energy (and, hence, the kinetic energy of separation) is 175 MeV. If the model is modified slightly to include a neck between the two nuclei, increasing the distance between the charge centers to 13.5 fm, the kinetic energy would be 165 MeV, as experiment requires. Such an elongated shape with a small neck at the time of separation in fission (the "scission" shape) is supported by several types of evidence.

The remaining ~ 23 MeV of fission energy is retained in the fission product nuclei as internal excitation and mass energy. This energy is released in a sequence of β-decay steps in which the *N/Z* values are adjusted to stability. Table 14.1 summarizes the distribution of fission energy.

TABLE 14.1. *Data for energy distribution in thermal fission of* ^{235}U *in MeV*

Prompt energy			176.5 ± 5.5
of which the	kinetic energy of fission products	164.6 ± 4.5	
	kinetic energy of 2.5 prompt neutrons	4.9 ± 0.5	
	γ-energy (prompt)	7.0 ± 0.5	
Delayed energy from fission product decay			23.5 ± 5.0
of which the	kinetic energy of β's	6.5 ± 1.5	
	neutrino radiation	10.5 ± 2.0	
	γ-energy	6.5 ± 1.5	
Total			200.0 ± 6
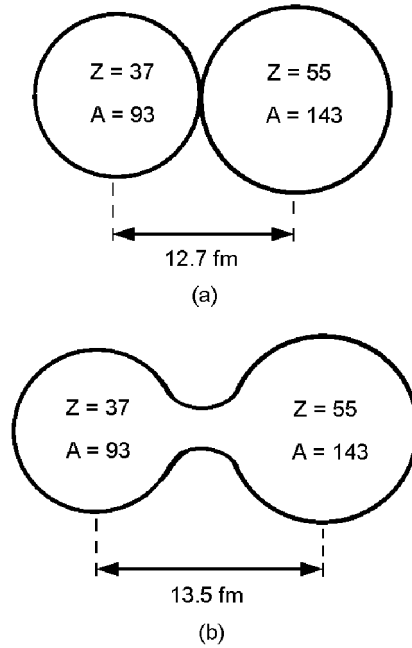
FIG. 14.12. Fission of ^{236}U showing the distance between the effective centers of charge. (a) touching spheroids, (b) a scissioning dumbbell. Nuclear radii are calculated by $r = A^{1/3}$.

14.7.3. *Fragment kinetic energies*

In fission induced by thermal neutrons (or spontaneous fission) the fissioning nucleus has a low kinetic energy. Thus the fragment kinetic energies are very near the same in the laboratory coordinate system and in the center-of-mass system. During fission, the center of mass must remain stationary and the total impulse must be zero. Assuming $A \propto m$, the fragment kinetic energy, E_1, of a fragment with mass A_1 is given by

$$E_1 = [A_2 / (A_1 + A_2)] \, E_{kin} \qquad (14.12)$$

where E_{kin} is the total kinetic energy of the two fission fragments and $A_1 + A_2$ is the mass of the fissioning nucleus. Hence the lighter fragment initially carries a larger part of the kinetic energy than the heavier fragment. The initial distribution of kinetic energy is distorted by the emission of energetic neutrons shortly after fragment separation. Fission fragments are often used when calibrating the energy scale of heavy ion surface barrier detectors. The number-averaged fragment energies in spontaneous fission of ^{252}Cf are 105.71 MeV for light fragments and 80.01 MeV for heavy fragments.

14.7.4. *Fission models*

The analogy between nuclei and liquid droplets was found to be useful in deriving the semi-empirical mass formula (§3.6). Bohr and Wheeler explained fission just months after its discovery by using the same model. The surface tension of a liquid causes a droplet to assume a spherical shape, but if energy is supplied in some fashion, this shape is distorted. If the attractive surface tension force is greater than the distorting force, the drop oscillates between spherical and elongated shapes. If, however, the distorting force becomes larger than the attractive force, the drop elongates past a threshold point and splits (fission).

In §3.6 we described how the repulsive forces between the protons in the nucleus could be expressed by a term a_c proportional to $Z^2/A^{1/3}$, and the surface tension attraction by another term a_s proportional to $A^{2/3}$. The repulsive Coulomb force tends to distort the nucleus in the same way a distorting force does a droplet, while the surface tension tries to bring it in to a spherical form. The ratio between the two opposing energies should measure the instability to fission of the nucleus. As shown in §11.7.4, the liquid drop model predicts that the probability of fission should increase with increasing Z^2/A. Of all naturally occurring nuclides only ^{235}U can be fissioned by thermal neutrons, while ^{238}U fission requires energetic neutrons ($\geq$ 2 MeV). With increasing Z (> 92) the fission probability with thermal neutrons increases and the half-life of radioactive decay by spontaneous fission decreases. Both of these processes are more probable for even Z-elements than for odd Z-elements. The half-life for spontaneous fission decay is given in Figure 14.13 as a function of the fissionability parameter, x.
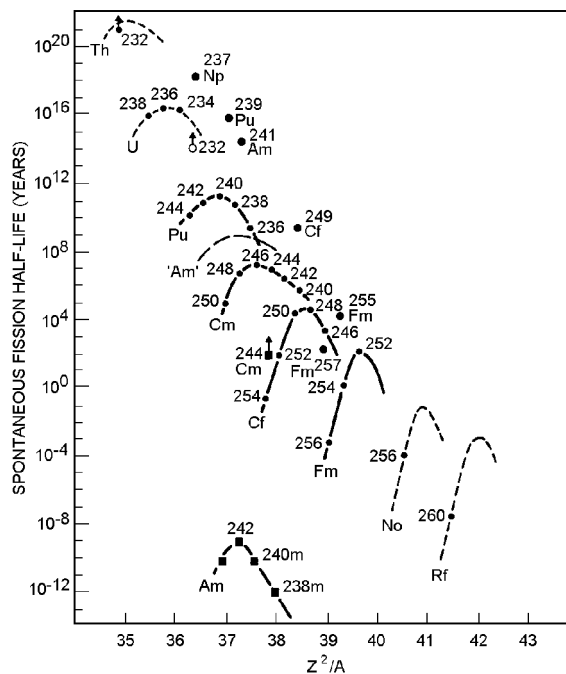
FIG. 14.13. Spontaneous fission lifetimes. (From Strutinsky and Bjørnholm.)

In the semi-empirical mass equation a spherical shape is assumed. If *N* and *Z* are kept constant and the potential energy of the nuclear liquid drop is calculated as a function of deformation from spherical to prolate, the curve in Figure 14.14a is obtained. The nucleus exists normally in the ground state level of the potential well. In order to undergo fission it must be excited above the fission barrier which is about 5 - 6 MeV. As the diagram shows, this means excitation of the nucleus into the continuum level region if the nucleus retains the shape associated with the potential well. However, if the nucleus deforms, some excitation energy goes into deformation energy. At the top of the barrier, the nucleus is highly deformed and has relatively little internal excitation energy. It exists in well-defined vibrational levels, and fission occurs from such a level. This is known as the "saddle point" (the top of the barrier) of fission.

It has long been recognized that the liquid-drop model semi-empirical mass equation cannot calculate the correct masses in the vicinity of neutron and proton magic numbers. More recently it was realized that it is less successful also for very deformed nuclei midway between closed nucleon shells. Introduction of magic numbers and deformations in the liquid drop model improved its predictions for deformed nuclei and of fission barrier heights. However, an additional complication with the liquid-drop model arose when isomers were discovered which decayed by spontaneous fission. Between uranium and
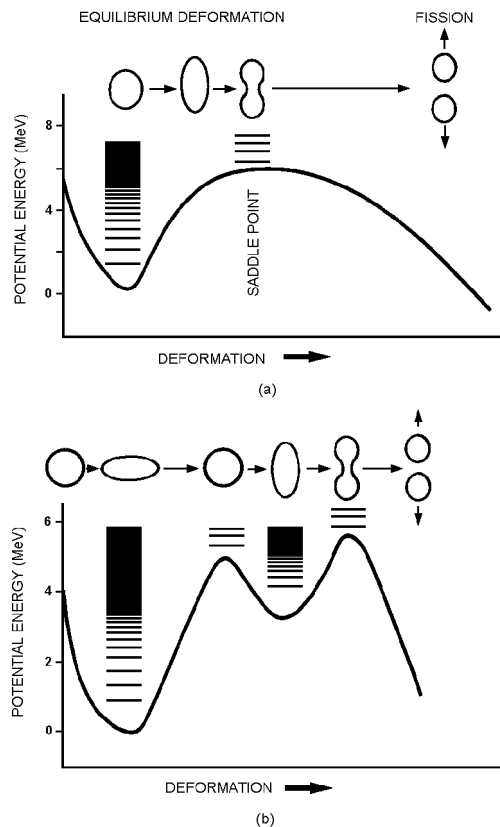
FIG. 14.14. (a) The liquid-drop model potential energy curve. (b) Same, but modified by shell corrections.

californium a number of nuclides were found to decay by spontaneous fission with half-lives of 10^{-2} to 10^{-9} s, millions of times slower than prompt fission which occurs within 10^{-14} s but millions of times faster than normal spontaneous fission (Fig. 14.13). For example, ^{242}Cm has a ground state half-life to spontaneous fission of 10^{6} years, while an isomeric state of ^{242}Cm has been found to fission with $t_{1/2}$ of 10^{-7} s.

Strutinsky developed an extension of the liquid drop model which satisfactorily explains the fission isomers and asymmetric fission. For such short half-lives the barrier must be only 2 - 3 MeV. Noting the manner in which the shell model levels vary with deformation (§11.5, the "Nilsson levels"), Strutinsky added shell corrections to the basic liquid-drop model and obtained the "double-well" potential energy curve in Figure 14.14b. In the first well the nucleus is a spheroid with the major axis about 25% larger than the minor. In the second well, the deformation is much larger, the axis ratio being about 1.8. A nucleus in the second well is metastable (i.e. in isomeric state) as it is unstable to γ-decay to the first well or to fission. Fission from the second well is hindered by a 2 - 3 MeV barrier, while from the first well the barrier is 5 - 6 MeV, accounting for the difference in half-lives.

The single-well curve in Figure 14.14a predicts symmetric fission whereas the double-well curve (Fig. 14.14b) leads to the correct prediction of asymmetric fission and a thin neck. Incorporation of shell effects in the fission model also leads to the prediction that the half-lives of very heavy nuclides ($Z \geq 106$) must be longer than the simple liquid-drop model would indicate. This has led to a search for "super heavy" elements with $Z = 110 - 118$.

14.8. Photonuclear reactions

If a photon transfers sufficient energy to a nucleus to excite it to a higher state, three possibilities for de-excitation exist: (a) the same energy is immediately re-emitted isotropically, (b) a long-lived isomer may be formed which decays through emission of one or more γ-rays, and (c) the nucleus disintegrates. The first process (a) is referred to as the Mössbauer effect and is discussed in chapter 6. The second process (b) of nuclear de-excitation has been discussed earlier. The third process (c) is referred to as *photonuclear disintegration.* The energy transferred to the nucleus must be sufficient to excite it above the dissociation energy for a proton, neutron, or other particle. A large energy transfer can also induce fission of heavy nuclei, *photo fission.*

The simplest photodisintegration process is that of the deuteron, whose binding energy is 2.23 MeV. If the γ-ray energy absorbed exceeds this value, a neutron and a proton are formed. This is a common reaction in nuclear reactors using heavy water as moderator, because the fission γ-ray energy is often several MeV. However, γ-rays of such energy rarely occur in the radioactive decay of nuclides (i.e. with half-lives of hours or longer). The cross-section for photodisintegration of ^{2}H has a maximum value of 2.4 mb at 4.3 MeV E_γ.

The energy necessary for photodisintegration of a nucleus is calculated from known nuclear masses. It is obviously easier to remove one particle than several from a nucleus. As a result we find that E_γ must be ≥ 5 MeV for photodisintegration of heavier nuclei.

For 10 E_γ 40 MeV the photon wavelength is comparable to the nuclear size. It is therefore easily absorbed, which causes collective nuclear vibrational motions (so-called dipole vibrations, because the neutrons and protons are assumed to vibrate in separate

groups). De-excitation occurs through γ-emission. This is known as the "giant resonance" region, because the total cross-section for heavier nuclides goes up to hundreds of millibarns. For higher E_γ, nucleons may be expelled, the main reactions being (γ,n), (γ,2n) and (γ,np) in order of descending importance. As the γ-energy increases and the wavelength decreases to nucleon dimensions, interaction with nuclear groups (e.g. deuterons) or single nucleons takes place. Below 550 MeV one pion plus a nucleon may be emitted in the de-excitation following the photon absorption. At higher energies, several pions may be emitted. Very little is known about the details of these processes.

14.9. Exercises

14.1. A 0.01 mm thick gold foil, 1 cm^2 in area, is irradiated with thermal neutrons. The (n,γ) cross-section is 99 b. What is the transformation rate at a n-flux of 10^{19} n m^{-2} s^{-1}?

14.2. Assume the irradiation time of the gold foil in the previous problem is one week. What percentage of the original gold atoms in the target have undergone transformation?

14.3. A water-cooled copper foil (0.1 mm thick) is irradiated by the internal beam of a sector focused cyclotron with 1.2 mA H^+ ions of 24 MeV for 90 min. The reaction $^{63}Cu(p,pn)^{62}Cu$ occurs with a probability of 0.086 b. Copper consists to 69% of ^{63}Cu. The proton beam has a cross-section of only 15 mm^2. (a) How many ^{62}Cu atoms have been formed? (b) What fraction of the projectiles have reacted to form ^{62}Cu? (c) What cooling effect is required (kW) at the target?

14.4. Calculate the macroscopic cross-section for reaction of natural uranium with thermal neutrons. See Figures 16.1 and 19.5.

14.5. (a) Estimate the yield (% of fissions) of ^{142}La in thermal fission of ^{235}U given a chain yield of 5.839% for A = 142, most probable charge = 55.86 and a width parameter of 0.56. (b) Is an appreciable amount of ^{142}Nd formed directly in thermal fission of ^{235}U?

14.6. The total kinetic energy of the fragments from thermal fission of ^{239}Pu is 177.7 MeV and the average fragment masses are 100.34 and 139.66 u respectively. What are the kinetic energies of the average light and heavy mass fragments?

14.7. Calculate the kinetic energy of the ^4He ion formed through thermal neutron capture in ^{10}B.

14.8. What is the minimum photon energy required for the reaction $^{11}B(\gamma,n)^{10}B$?

14.9. A 2 MeV neutron collides elastically with an iron atom (^{56}Fe). What is the average temperature (corresponding to the maximum velocity) which can be ascribed to the iron nucleus after the collision?

14.10. Literature

P. M. ENDT and M. DEMEUR, *Nuclear Reactions*, North-Holland, 1959.

V. GOLDANSKII and A. M. BALDWIN, *Kinetics of Nuclear Reactions*, Pergamon Press, Oxford, 1961.

Physics and Chemistry of Fission, IAEA, Vienna, 1965, 1969, and 1973.

V. S. FRASER and J. C. D. MILTON, Nuclear fission, *Ann. Rev. Nucl. Sci.,* **16** (1966) 379.

M. LEFORT, *Nuclear Chemistry*, van Nostrand, 1968.

R. VANDENBOSCH and J. R. HUIZINGA, *Nuclear Fission*, Academic Press, 1973.

K. WOLFSBERG, *Estimated Values of Fractional Yields from Low Energy Fission and a Compilation of Measured Fractional Yields*, Report LA-5553-MS, UC-34c, Los Alamos Scientific Lab., May 1974.

R. VANDENBOSCH, Spontaneously fissioning isomers, *Ann. Rev. Nucl. Sci.,* **27** (1977) 1.

Nuclear Structure Physics, ed. S. J. HALL and J. M. IRVINE, Proc. 18th Scottish U. Sum. Sch. in Physics, Edinburgh, 1977.

D. C. HOFFMAN, T. M. HAMILTON and M. R. LANE, *Spontaneous Fission*, Report LBL-33001, UC-413, Lawrence Berkeley Lab., Oct. 1992.